Synthesis and characterization of novel dendritic macroporous monoliths

Sergio David García Schejtman, Cecilia Inés Alvarez Igarzabal, Marisa Martinelli*

Universidad Nacional de Córdoba, Facultad de Ciencias Químicas, Laboratorio de Materiales Poliméricos (LaMaP), Córdoba, Argentina
Instituto de Investigación y Desarrollo en Ingeniería de Procesos y Química Aplicada (IPQA), CONICET, Córdoba, Argentina

A B S T R A C T

The monoliths have changed the paradigm of the supports for applications in different fields, such as chromatography, catalysis, combinatorial chemistry, enzymatic bioreactors, among other. Particularly, the dendronized monoliths are a good alternative of hybrid material due to multivalency. Dendronized macroporous monoliths were prepared from a Newkome-type dendron (Beherás amine) and classical monomers such as NAT, AAm, AAc, and (BIS) as cross-linker. The monoliths have been thoroughly characterized using infrared microscopy, scanning electron microscopy (SEM), thermogravimetric analysis and swelling index. For the reaction, several factors such as monomer, solvent, porogen and their ratios were analysed. The morphological characteristics of monoliths were mainly managed by the conditions of the synthesis way, offering the opportunity to tailor pore size, surface characteristics and porosity. The results demonstrated a compromise between both the dendronized degree and the dynamic in the formation of globules and clusters during the polymerization reaction. It was also demonstrated that the porosity properties were governed by the dendritic moiety of the monoliths.

1. Introduction

The advances in the last years referred to the synthesis in solid phase, catalysis and different types of extraction and/or separation methodologies have aroused interest regarding the development of new polymeric materials to be used as supports. Precisely in the last 60 years the support polymeric materials have advanced from simple three-dimensional polymers [1] to products with strict control of properties, both chemical and morphological [2].

Currently, a particular class of materials that attract attention are the macroporous polymers, whose structure are characterized by a permanent porosity, formed during the preparation of the material, which keeps even in dry state. The internal structure is constituted by aggregates of microglobules of the polymeric chains interconnected by pores and their rigidity is due to the high degree of cross-linking [3]. These macroporous materials can be bead-type, obtained from a suspension polymerization, or monolithic type bars.

Particularly, the monoliths have changed the paradigm of stationary-phase design [4] enabling efficient separation, although in the last years have found various applications [5] including solid phase extraction SPE, supports for combinatorial chemistry, high throughput enzymatic bioreactors, or even as substrates for surface-enhanced Raman scattering. Monolithic materials are based on crosslinking macroporous polymer networks or on functionalized silica derived from

sol-gel synthetic path [6]. The monoliths are not expandable, and show interstitial spaces and large void volume, with good mechanical properties (stable), biocompatibility, high porosity, chemical resistivity and access sites for ligand-target interaction (covalent or non-covalent bond) [7]. Essentially, the pores in any monolith prepared by a polymerization with porogenic agents are known as macropores (voids between clusters, greater than 50 nm), mesopores (voids between the globules in clusters, 2–50 nm) and micropores (voids within globules, less than 2 nm) [8].

Crosslinked polymeric networks synthesized by combining different monomer types can give specific physicochemical properties to the material. Various support materials used as stationary phases in affinity chromatography are macroporous polymer monoliths due their appropriate characteristics for separation of macromolecules. Arrua et al. reported the preparation of affinity chromatography supports based on macroporous monoliths, synthesized by free-radical polymerization from *N*-[tris(hydroxymethyl)methyl]acrylamide (NAT) with *N,N'*-methylenebisacrylamide (BIS) or trimethylolpropane trimethacrylate (TMPTMA) as crosslinkers [9]. In all cases, experimental conditions such as temperature, monomer ratio and porogenic mixture were evaluated. Several authors also reported monoliths from styrene and divinylbenzene for chromatographic separations [10–12]. However, the preparation of monoliths with good performance for purification of macromolecules (DNA, proteins, and enzymes) is in continuous

---

development [4,13–17].

A further challenge is the use of branched polymers or dendrimers for the monomer design since recognition processes are significantly enhanced by multivalent interaction. Multivalency is likely to originate from the cooperative effect of specifically located multiple ligands. Nature uses multivalent receptors in different recognition processes to facilitate and enhance ligand-receptor interaction [18,19]. The multivalent effect may be caused by both the synergetic effect of locating multiple receptors or by an aggregation process. Because of their highly-branched structure, dendritic molecules are ideal to design novel supports for different applications. Dendritic structures are monodispersed, structurally perfect with high molecular weight, with a point of ramification in each monomeric unit, starting from a multifunctional core. These structures have strict control of the molecular architecture and great structural complexity. In the outermost part, they show high density of functional groups that can be modified to control the properties of the resulting macromolecule [20]. One of their central properties is the so-called dendritic effect, which directly depends on the generation. If all the generations of dendrimers have the same effect, this is called multivalency; yet, if the effect varies with generations, this is called generation effect [21,22]. Our group described the use of the dendronization process to obtain chitosan and gelatine microspheres and films. The products improved their mechanical properties, and the dendritic effect was evidenced in the rugosity, polarity in the interaction with other molecules, among others [23–26]. We also reported the preparation of functionalized supports with a sugar dendritic ligand on poly (hydroxylated polybutadienic-hydroxyethyl methacrylate) [27]. First, the dendritic molecule was immobilized on the matrix and then submitted to react with glucose. Finally, the glucose-containing supports were used as sorbents to retain Concanavalin A. We concluded that the topological nature (architecture and size) and the chemical nature of the dendron governed the multivalent effect. One important point is that in all cases, the properties discussed for each dendron-containing system were achieved using low dendron concentration, which further justifies its use and advantages of the dendronization processes.

Accordingly, novel and alternative dendritic-based hybrid polymers that synergistically combine the benefits and properties of macroporous polymer monoliths and hyperbranched molecules can be obtained. Various parameters such as temperature, polymerization time, type of monomer, monomer-porogen ratio and concentration can be studied to analyse the porosity, morphology, physicochemical properties, hydrodynamic and mass transfer characteristics of the monolithic support.

The dendronization methodology is a good alternative of hybrid material synthesis ideally suited as a synthetic tool for achieving interesting dendritic structures [28]. The use of dendrons as building blocks, allows the process to lower the number of reaction steps and reduces the need of tedious purification procedures.

Nowadays, monolithic polymers are enjoying a lot of interest among the research groups worldwide [15,17,29]. Most attractive areas include use of less common combinations of monomers that provide the monolithic structures with some new properties. Use of a dendritic monomer is rather unusual in the preparation of separation media in chromatography in general and in the field of monoliths in particular [22]. This manuscript aims at the preparation of monoliths using dendronized acrylamide copolymerized with hydrophilic monomers.

Hence, a dendritic macromonomer (DM) from a commercial dendron was synthesized, obtaining different macroporous monoliths from DM and classical monomers such NAT, acrylamide (AAm) and acrylic acid (AAc), and BIS as crosslinker. Certain aspects of the behaviour of multibranched molecules (dendrons) are dominated by structural and geometric features since functionality on the surface (polar or nonpolar) and architecture/size define their final properties. To facilitate a wide range of bio-screening applications, this article also discusses different process conditions to establish the multifunctional and macroporous properties of dendritic monoliths.

2. Materials and methods

2.1. Materials

Di-tert-butyl 4-amino-4-(3-(tert-butoxy)-3-oxopropyl)heptanedioate (aminotriester, Behera's amine) was purchased from Frontier Scientific (USA) and used as received; benzoyl chloride was purchased from Merk and used as received; AAc (99%, anhydrous, contains 200 ppm of methyl hydroquinone as an inhibitor), triethylamine (TEA, 99.5%), NAT (93%, contains ≤ 7% KCl), AAm (98%), BIS (99%) and 2,2′-azobis(2-methylpropionitrile) (AIBN, 98%) were purchased from Sigma-Aldrich (USA); polyethylene glycol Mw = 6000 (PEG 6000, Fluka), ethanol, *n*-pentanol, dodecanol ($C_{12}H_{25}OH$, Fluka), tetradecanol ($C_{14}H_{29}OH$) were used as co-porogens; all solvents were previously distilled and/or dried using molecular sieves (4 Å 8–12 mesh) (Sigma, USA).

AIBN was purified by recrystallization from methanol and used within two months. AAc was purified by distillation under reduced pressure.

2.2. Synthesis of acrylate Behera's amine (ABA): dendritic monomer

Acryloyl chloride was synthesized from AAc and benzoyl chloride. The method to obtain an acrylamide group from the commercial amine dendron (Behera's amine) has been reported [30]. Briefly, to a stirred solution of the dendron (2.0250 g, 4.9 mmol), TEA (1.2 mL, 8.5 mmol) in dry CH_2Cl_2 (40 mL) at 0 °C, acryloyl chloride was added dropwise (0.5 mL, 6 mmol) in CH_2Cl_2 (8 mL), stirring for additional 24 h at room temperature. After reaction, the mixture was washed with water and saturated brine. The organic phase was dried with $MgSO_4$, filtered and concentrated at vacuum to yield a yellow solid. The product was then purified using column chromatography (SiO_2, EtOAc/$CHCl_3$ 1:9 v/v) to obtain ABA (95%) as a white solid (2.1861 g). ^1H NMR ($CDCl_3$) δ (ppm) 1.43 (s, 27H); 2.03 (t, J = 7.7 Hz, 6H); 2.25 (t, J = 7.7 Hz, 6H); 5.58 (dd, J = 10.2, 1.0 Hz, 1H); 6.03 (dd, J = 16.9, 10.2 Hz, 1H); 6.21 (s, 1H) and 6.26 (dd, J = 5.0, 0.5 Hz, 1H); ^{13}C NMR ($CDCl_3$) δ (ppm) 28.2; 29.8; 30.1; 57.9; 80.7; 126.2; 132.0; 165.1 and 173.2; FT-IR (cm^{-1}) 3307; 2973; 1727; 1660; 850 and 757 (^1H and ^{13}C NMRs spectra are shown in Supplementary Data, Figs. S1 and S2, respectively).

Supplementary data associated with this article can be found, in the online version, at https://doi.org/10.1016/j.eurpolymj.2018.07.008.

2.3. Synthesis of macroporous dendritic monoliths

Different dendritic monoliths were synthesized from ABA as a dendritic monomer, BIS as a crosslinker and NAT, AAm and AAc as co-monomers. To obtain different systems, the ratio and nature of monomers and solvent:porogen ratio were changed. All samples were prepared by free-radical polymerization using a polypropylene syringe (0,9 cm of diameter) as a reaction mold. First, monomers were dissolved in 1 mL of porogenic mixture (solvent:porogen 70:30). The mixture was stirred at 60 °C until complete dissolution and then purged with N_2. Then, radical initiator AIBN was added (1% with respect to monomers) and the reaction was carried out for 24 h at 70 °C. After reaction, polymers were washed with methanol using a soxhlet equipment for 48 h. Products where dried under vacuum to give different white monoliths (yield 90–95% with respect the total mass of monomers).

2.4. Physicochemical characterization

The NMR spectra were carried out using a Bruker UltraShield 400 (400 MHz and 100.6 MHz for ^1H y ^{13}C, respectively) equipment. FT-IR spectra were performed using a Nicolet iN10 equipment (Thermo Scientific, USA) (ST 2425-CONICET) with mercury cadmium telluride (MCT) detector and OmnicPicta workstation. Spectra were collected in high-resolution (8 cm^{-1}) mode and 64 scans. The samples were

deposited on a gold mirror.

The surface morphology of the polymers was analysed by scanning electron microscopy (SEM) using a SEM Carl Zeiss Sigma equipment with EDS (OXFORD-AZTEC XMAX 80) (LAMARX, FaMAF-UNC). SEM images were acquired at magnifications between 5000 and 20,000X or well the width of the image field was between 15 and 60 μm (Figs. S3–S15), to visualize the fine pore structure of different regions of each sample. The average size of monolith pores and the distribution of pore sizes in drying state were obtained based on calculating about 100–150 pores. All samples were sputter-coated with gold before taking images. ImageJ 1.51k free software was used for the pore size measurements. Specific surface area was determined by the Brunauer–Emmet–Teller (BET) method [31] using a Micromeritics Tristar II 2020 automated nitrogen sorption–desorption instrument (ACROSS, Australia). Prior to analysis, all samples were dried in a Micromeritics SmartPrep at 70 °C for 24 h. Thermal degradation curves of monomers and polymers were performed on a Shimadzu DTG-60 (Japan) (ST 2901-CONICET), over a temperature range of 30–600 °C at a heating rate of $10\,°C\,min^{-1}$ in nitrogen atmosphere. Mass variation in the swelling behaviour was studied using deionized water and DMSO, measured on a Mettler Toledo Newclassic MF balance (Model MS204S). Samples (40–50 mg) were weighted in dry state and swelled in water or DMSO for 24 h in a beaker. The equilibrium swelling degree was afterwards determined using the following equation:

$$Swelling\,(\%) = \frac{W_e - W_d}{W_d} \cdot 100 \tag{1}$$

W_d and W_e are mass of the sample in the dry state and in the equilibrium of swelling, respectively.

3. Results and discussions

The goal of this work was to rationally design dendritic polymer-based monoliths that can be used as supports in different fields. Thus, the monoliths could show optimal selectivity and affinity constant to the ligands, due to the cooperative effect of the dendritic moiety [32]. To achieve this, a Newkome-type dendritic monomer bearing three tert-butyl groups, ABA, was used as co-monomer. The functionality of DM could considerably modify the properties of the polymer. The tert-butyl groups generate a more hydrophobic environment, but by different reactions, new functional groups can be obtained, such as amino groups (by transamination) or acid groups (by hydrolysis/thermolysis) [33–35]. As the same way, different classical monomers were used, such NAT, AAm and AAc.

3.1. Synthesis of dendritic monomer and macroporous dendritic monoliths

At a first synthetic stage, the dendritic monomer ABA was prepared by a slightly modified protocol, previously reported by our group [33]. The first step involved acrylation of the commercially available Behera's amine with acryloyl chloride. ABA includes an acrylamide group as focal point (Scheme 1) and the capability to react through free radical polymerization. ^{1}H NMR confirmed the acrylated product by the
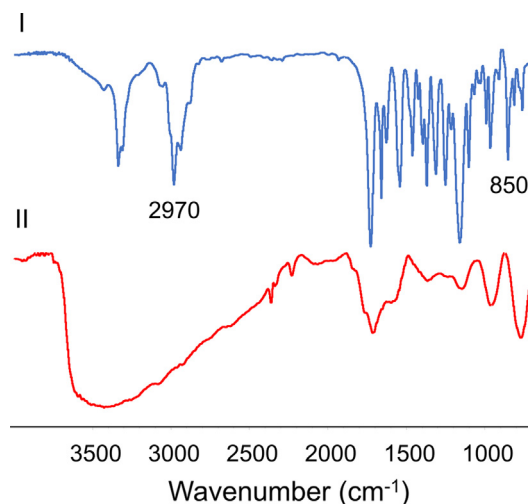

Fig. 1. FT-IR spectrum of (I) ABA and (II) ABA after heating at 250 °C.

peaks assigned to vinyl group at 5.58, 6.03 and 6.26 ppm ($H_2C{=}CHR$) and the approach of a methylene signal of dendron from 1.65 to 2.03 ppm. The ^{13}C NMR also confirmed acrylation by the new peak assigned to the amide group at 165.1 ppm (C=O) and the presence of vinyl carbons at 126.2 and 132.0 ppm ($H_2C{=}CHR$). Infrared spectrum (Fig. 1I) showed two signals at 1727 and 1660 cm^{-1} corresponding to stretching C—O of carbonyl ester group and carbonyl amide group (amide I), respectively. The expected two highlighted signals at 850 and 757 cm^{-1} corresponding to deformation of tert-butyl groups and the tight signal at 2970 cm^{-1} corresponding to stretching of C=H sp[3], were also used to confirm the dendron incorporation in the polymer [25].

The mechanism of formation of macroporous polymer monoliths was already described [2,36,37]. Briefly, the process begins with the formation of nuclei resulting from free radical reactions. These particles are the seeding nuclei for the formation of microglobules, which aggregate and precipitate out of the solution to form the polymer. The formation of irregular pores and the interconnectivities are driven by the coagulation of microglobules and their aggregates. Then, this process defines the pore characteristics of the polymer with the geometric shape of the mold reaction. The separation of phase seems to be determining to improve the pore characteristics that depend on several factors: monomer, solvent, porogen, temperature and initiator, among others [37]. Different conventional systems using dendron as a monomer (or co-monomer) were used to evaluate the characteristics of the monoliths by the presence of the dendritic molecule.

Monoliths were prepared by free-radical crosslinking polymerization to yield different polymer networks as shown in Table 1. The systems involve different types of monomers: functional classical monomer, functional dendritic monomer (DM) and crosslinker, as shown in Scheme 1.

The polymer names are based on monomers used: NAT-BIS, NAT-ABA-BIS, ABA-BIS, AAm-BIS, AAm-ABA-BIS, AAc-BIS and AAc-ABA-
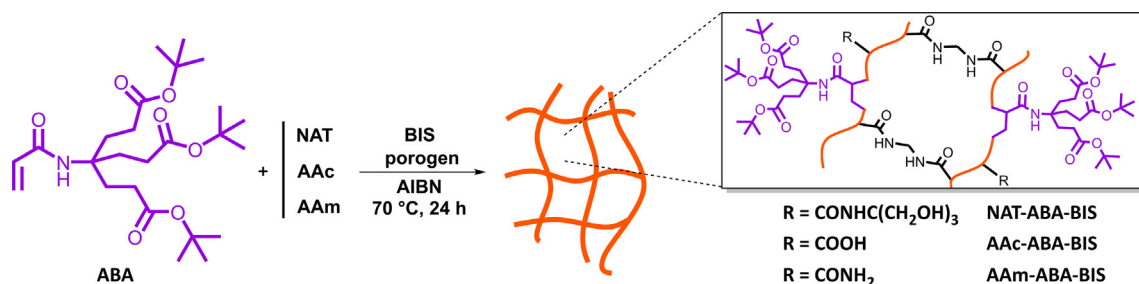
Scheme 1. Synthetic route to obtain dendronized co-polymers as monolith rods.

Table 1
Different matrices obtained from NAT, ABA and BIS[a].

Matrix	NAT (%)	ABA (%)	BIS (%)	Pore size (nm)	Yield (%)	Dendron incorporation (%)[b]
NAT-BIS	60	0	40	600 ± 100	98.3	–
NAT-ABA20-BIS	40	20	40	1100 ± 200	90.2	90.3
NAT-ABA30-BIS	30	30	40	1400 ± 300	98.2	88.0
NAT-ABA40-BIS	20	40	40	400 ± 100	95.3	95.1
ABA60-BIS	0	60	40	330 ± 70	89.7	90.2
ABA50-BIS	0	50	50	< 300		
ABA20-BIS	0	20	80			

[a] Polymerization conditions: monomer concentration: 2.8 M. AIBN: 1% w/w with respect to total of monomers. Polymerization time: 24 h; temperature: 70 °C; DMSO:co-porogen (%vol): 70:30 with respect to total volume of the porogenic mixture equal to 1 mL. Co-porogen: PEG6000:tetradecanol (50:50).
[b] Percentage of the mass lost from TGA graphical.

BIS. In all cases, monoliths that were obtained with high yield contain pores larger than 50 nm (macropores), maintaining their porosity in dry/swollen state (Table 1). However, many products were highly brittle, such as ABA-BIS (in all dendron concentrations).

The monomers contribute to the rod with different physicochemical properties; their type and ratio allow controlling porosity in the products. In general, the concentration of the crosslinker affects the pore size, pore volume and permeability [38,39]. If the concentration of the crosslinker is high, an increase in covalent interconnectivities is found between nuclei, resulting in small pore size and low porosity. According to previous studies [9] and the results of the pore size (Table 1), the optimal concentration of crosslinker was 40%.

The FT-IR spectra of NAT-based matrices (Fig. 2) show different characteristic signals: 3670–3580 and 3460–3420 cm^{-1} (−OH and −NH stretching vibrations, respectively), 1680–1630 cm^{-1} (C−O stretching vibrations, amide band I); 1570–1515 and 1305–1200 cm^{-1} (combination bands of N−H deformation and C−N stretching vibrations, amide bands II and III, respectively); 1280–1260 and 1075–1000 cm^{-1} (C−O stretching and O−H in-plane deformation of primary alcohol). The dendron incorporation was controlled by FT-IR, where the signals at 850 and 757 cm^{-1} correspond to tert-butyl groups of the dendritic surface and the signal at 1726 cm^{-1} corresponds to carbonyl dendron group. It was clearly observed that the relative intensity of these signals increased with the amount of dendritic monomer.

Furthermore, the incorporation of ABA into the matrices was also proved by thermogravimetric analysis as shown in Fig. 3. The thermal decomposition of dendritic monomer (Fig. 3A) at 225 °C corresponds to the mass loss of tert-butyl groups [34,40]. When the amount of ABA to the matrices increased, the mass lost at 225 °C was also increased (Fig. 3B). Moreover, if the dendritic monomer loses 37% of mass, the percentage of mass lost at 225 °C in the matrix represents the amount of dendritic monomer incorporated. Knowing the initial mass of the monomers, the molar mass of the dendron and the percentage of the mass lost from TGA graphical, it is possible to estimate the incorporation of the dendritic molecule in the monolith (Table 1). The FT-IR spectrum of the residue obtained at 250 °C (Fig. 1II) also proved the disappearance of the signals at 850 and 757 cm^{-1} corresponding to the dendron (see Fig. S16 for TGA-DTG curves of each polymer). Thus, all matrices showed an effective incorporation of dendritic monomer.

3.2. Optimization of polymerization condition

A microscopic analysis allows the observation that the formed pores in the matrices comprise asymmetrical voids between globules of the cluster, clusters of globules and intra-globular pores. Fig. 4 shows the
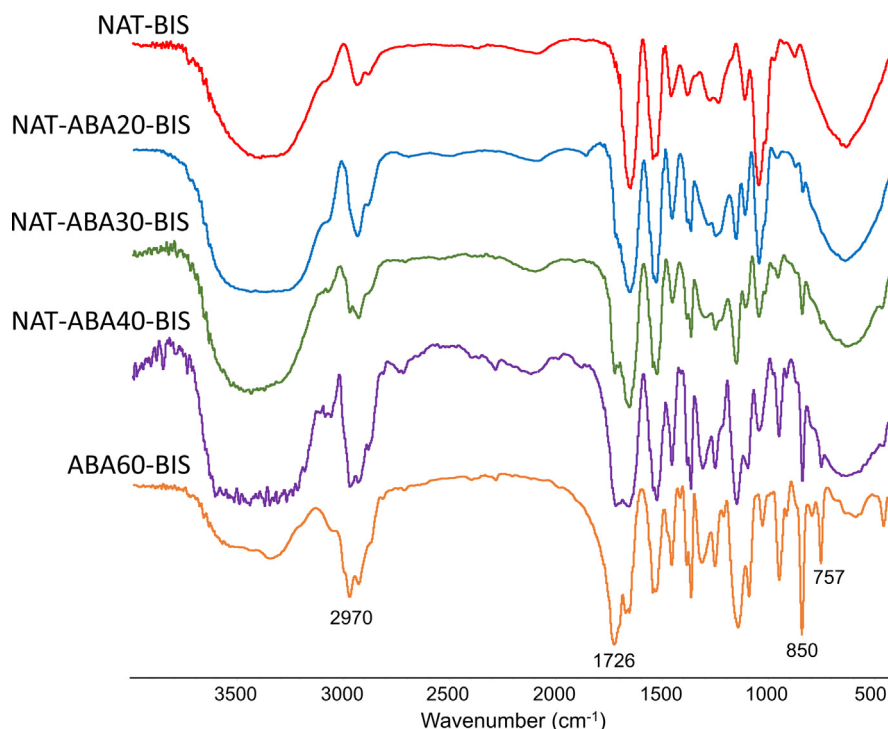

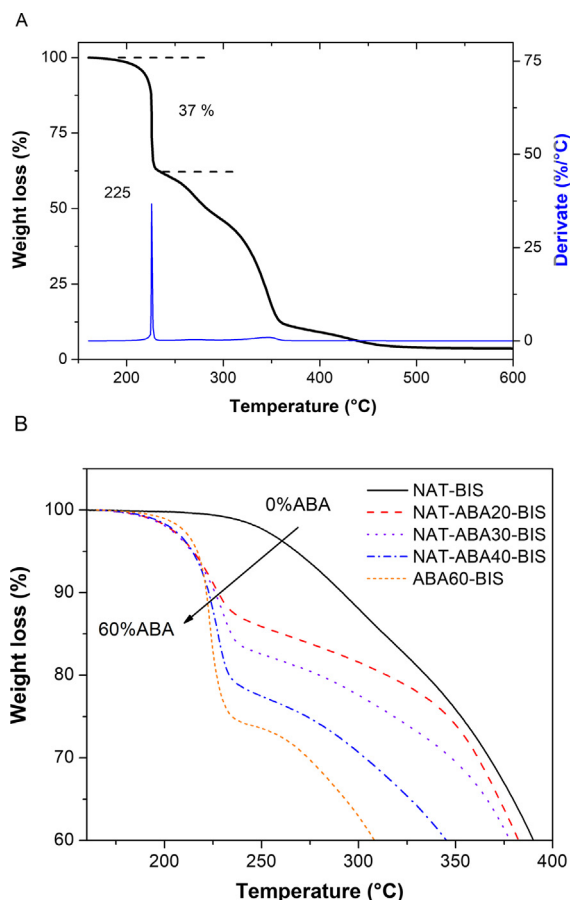Fig. 2. IR spectra of NAT-based and ABA60-BIS matrices.

Fig. 3. (A) TGA and DTG curves of ABA monomer. (B) Weight loss at 225 °C in TGA curve of different NAT-based matrices and ABA60-BIS.

images obtained by SEM, corresponding to the morphology of the different matrices.

Using NAT, the images show clearly aggregated microspheres in large clusters, between gaps of different size (pore) can be found. Furthermore, the distribution of macropore size and SEM images showed an increase of pore size when ABA percentage increased from 0 to 30%, and a major pore sizes dispersion in NAT-ABA30-BIS. The pore size decreased at higher concentration of dendritic monomer, in the same reaction conditions. This behaviour could indicate a compromise between the dendronized degree and the velocity of formation of globules and clusters during the polymerization reaction.

A high concentration of ABA (40%) results in a tight globular network with low pore size and volume. In addition, the synthesis of different ABA-BIS polymers was carried out, varying the mass ratio of ABA:crosslinker. It was concluded that the porous properties in the products of different relationships studied were different, since smaller size than that in NAT-ABA-BIS systems were observed, as shown in Table 1 (entries ABA50-BIS and ABA20-BIS) and SEM images (see Fig. S17).

In order to evaluate the effect of the dendron on micro and mesoporosity, nitrogen adsorption measurements of a non-dendronized material (NAT-BIS) and NAT-ABA20-BIS was determined and compared. The BET surface area and pore volume decrease from 11.23 to 7.73 $m^2 g^{-1}$ and 0.049 to 0.030 $cm^3 g^{-1}$, respectively, equivalent to the formation of denser microglobules attributed to two reasons: (i) the chains (using a dendritic structure) remain at a short distance or (ii) the formation of dense packing of dendrons leads to anchoring to the backbone [41,42].

The effect of the degree of dendron incorporation on the porosity of the monoliths can be understood as a contribution of steric and non-
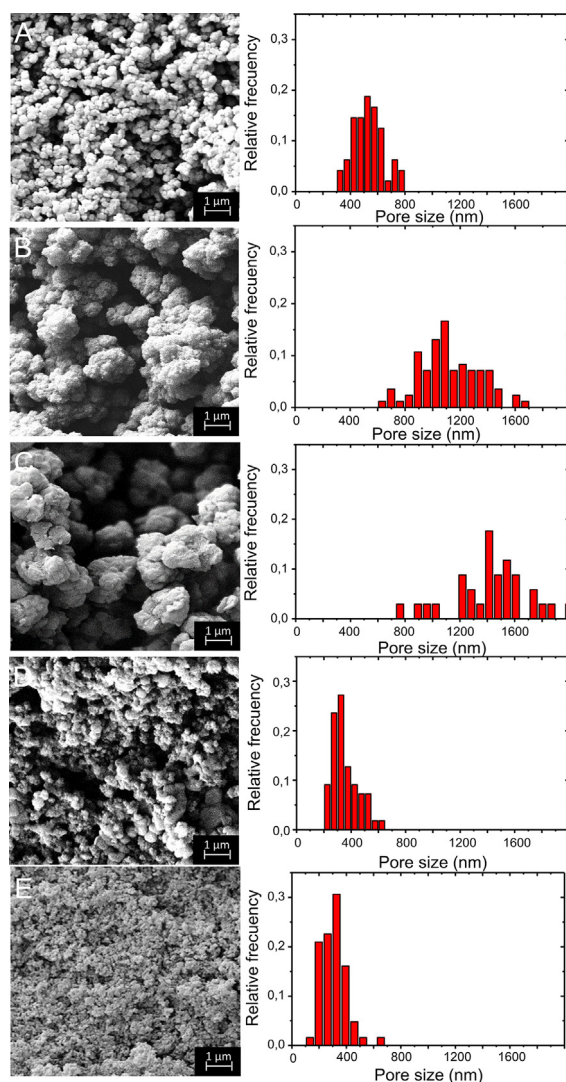

Fig. 4. SEM images and pore sizes distribution of (A) NAT-BIS, (B) NAT-ABA20-BIS, (C) NAT-ABA30-BIS, (D) NAT-ABA40-BIS, and (E) ABA60-BIS.

polar characteristics of ABA [40]. The non-polar properties predominate at lower concentration of dendron, giving large microglobules and large pore sizes due to early phase separation. At higher concentration of dendron, the steric effect is more important than the non-polar contribution, avoiding the growth of polymer chains and causing small microglobules and small pore sizes, even at early phase separation.

It is also clear that porosity properties are governed by the dendritic moiety of the monoliths. The presence of dendritic molecules could improve the macroporous properties even at low concentration.

The non-polar properties of ABA increased the hydrophobic structure of all polymers. This behaviour is shown in Fig. 5; the higher the ABA concentration, the lower the swelling in water. However, swelling in the reaction solvent (dimethyl sulfoxide) did not change significantly with dendron concentration.

The morphological characteristics of monoliths are mainly managed by the conditions of their synthesis way, and this offers the opportunity to tailor pore size, surface characteristics and porosity. As mentioned, the rate of polymerization and the properties of the monoliths depend on different variables. Generally, a solution of monomers, initiator and porogen(s) are placed in a temperature-controlled reactor to start the free radical copolymerization to form the polymer network. When the polymerization process ends, a heterogeneous system is formed: a
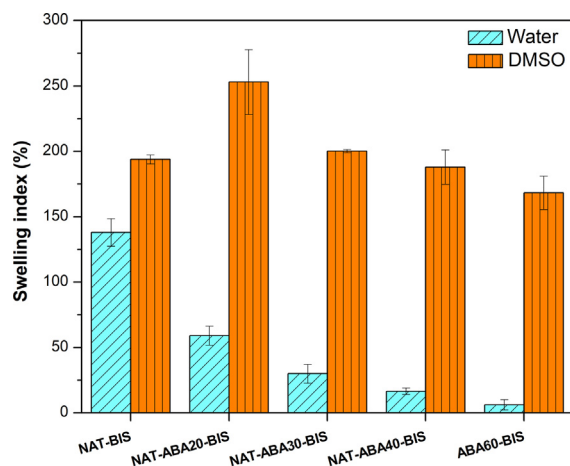
Fig. 5. Swelling percentage of NAT-based matrices in water and DMSO with different concentrations of dendritic monomer.

3.3. The effect of monomer functionality and concentration

To compare the effect of functional co-monomers, dendritic monoliths with AAc and AAm were obtained. AAc-ABA-BIS and AAm-ABA-BIS were obtained under the same reaction conditions analysed for ABA; however, poor yield and non-monolithic properties were reached (data not shown). Basically, a gel-like polymer was formed. For that, other reaction conditions (Table 3) were used for these systems, obtaining white solid monoliths with high yields. These novel dendronized polymers (AAc-BIS; AAc-ABA-BIS; AAm-BIS and AAm-ABA-BIS) were characterized as previously mentioned.

In AAc-based matrices, the incorporation of dendritic monomer can be observed from the signals at 844 and 757 cm^{-1}, corresponding to tert-butyl groups of the periphery stretching, as shown in Fig. 7. Solely, the FT-IR spectra of these matrices allowed estimate the dendronization degree by a measurement of the relative intensities of the signal at 844 cm^{-1} in relation to the signal at 956 cm^{-1} of BIS (Fig. 7B) (this is the only signal that remains constant in all products). The results agree with the ABA:BIS ratio (Fig. 7C).

The incorporation of ABA in AAm-based matrices was also proved by FT-IR spectroscopy (Fig. 8) but it could not be quantified because there is no distinguishable signal of BIS that remains constant. In addition to tert-butyl signals (2970, 845 and 755 cm^{-1}), the appearance of ABA carbonyl signal at 1720 cm^{-1} could be observed.

TGA-DTG curves (Figs. S18 and S19) were performed for each product. Fig. 9A and B show the derivative of weight loss of AAc and AAm-based matrices, respectively, and the increment of loss of ABA when the amount of dendron into the network increases. Thus, the incorporation of dendritic monomer was estimated and proved in Table 3, according to the same procedure for NAT-based matrices.

The behaviour of these matrices in water and DMSO was also compared. It was observed that AAc-based matrices (Fig. 10A) have less polar properties than AAm-based matrices (Fig. 10B). It might be caused by intramolecular hydrogen bonds due to the presence of carboxyl groups in AAc-based matrices. However, the incorporation of ABA decreased significantly the swelling in water. In all cases, the higher the concentration of ABA, the higher the hydrophobic properties of the final product, as seen with decrease in swelling in water and increase in DMSO. Thus, the influence of the non-polar characteristics of dendritic monomer was proved.

The dendronized monoliths with AAm and AAc showed similar morphological properties to NAT-based polymers, as shown in Fig. 11. The AAc-BIS system has a pore size distribution with a maximum of 700 nm (Fig. 11A). The presence of ABA by 20% significantly increases the pore sizes (Fig. 11B), where the distribution has a maximum at 1500 nm. However, when the percentage of dendron is greater than 20%, the pore sizes decrease (Fig. 11C), even reaching a distribution between 200 and 600 nm for the case of AAc-ABA40-BIS (Fig. 11D). Nevertheless, the advantage at high concentrations of dendron is related to a more homogeneous distribution.

AAm-based polymers were also studied. AAm-BIS presents morphological characteristics like AAc-BIS, with a distribution of pore sizes around of 800 nm (Fig. 11E). The presence of the dendritic monomer by 20% increase the distribution of pore sizes with a maximum between 1000 and 1500 nm. Although the increase of the concentration of ABA to 30% does not produce significant changes in terms of sizes, a significant decrease is observed when using 40%, when the maximum frequency values being around 500 nm. In these cases, more homogeneous distribution was also observed, because the presence of ABA.

The optimization of distribution of pore sizes by the presence of dendritic monomer were proved, even at lower concentration. It should be noted that the porous properties of AAm-based monoliths crosslinked with BIS reported in the bibliography are similar, under similar conditions [29,46–49]. The notorious advantage of the AAc-ABA-BIS and AAm-ABA-BIS matrices is mainly related to the multifunctionality granted by the dendritic structure, which are being evaluated.
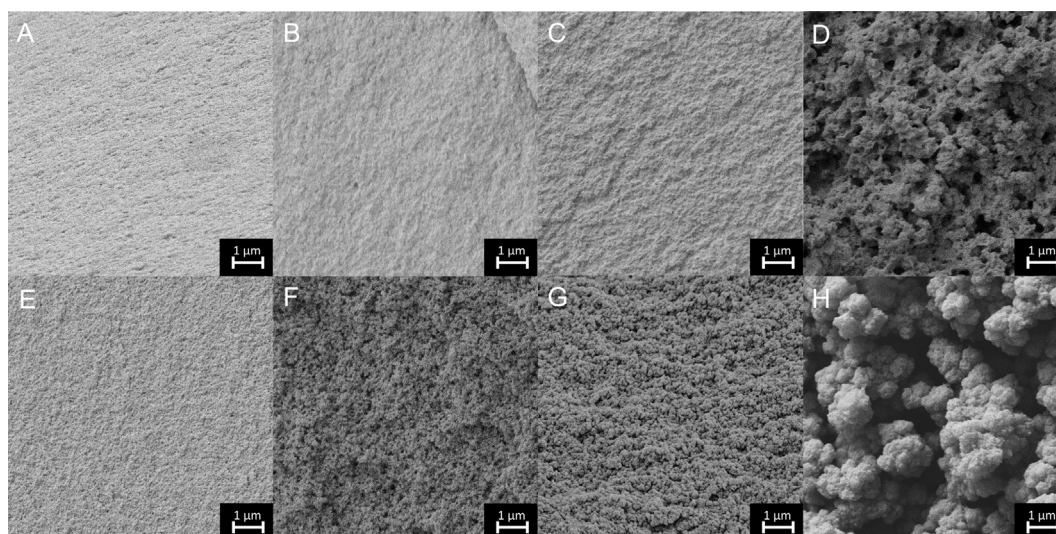
solution with porogenic mixture within the pores of continuous solid structure (monolith) [36,43]. The pore size of the monoliths formed could be controlled to range from micropores to macropores. Based on these considerations, different synthesis parameters were studied.

In the pore formation process, both the homogeneity and the phase separation process of the crosslinked nuclei and globules are affected by the properties of the porogenic mixture [38,44]. A solvating solvent, a non-solvating solvent, different alcohols, polymers or their combination are the porogenic agents more frequently used. Generally, the higher the porogen concentration, the higher the pore size distribution [7,45]. Alcohols with different chain lengths were used as non-solvating diluents for the synthesis of NAT-ABA20-BIS (Table 2) and the matrices were analysed by SEM (Fig. 6).

Ethanol and n-pentanol (Fig. 6A and B) were employed as porogens resulting good solvents for the separation of crosslinked nuclei, giving porosity lower than 100 nm. Dodecanol and tetradecanol (Fig. 6C and D, respectively) were used as macroporogens (porogens with high molecular weight and long aliphatic chain), increasing pore size up to 600 nm with tetradecanol, since its poor solvent property caused and early phase separation. In addition, PEG (Fig. 6E) was used as a polymer porogen nevertheless the porous properties were not improved. However, when tetradecanol:PEG 50:50 was used as co-porogen mixture [9] in DMSO, the pore size was up to 1000 nm, as shown in Fig. 6H.

DMAc, DMF and DMSO were used as solvents (Fig. 6F, G and H, respectively). Thus, high pore size was achieved using DMSO as solvent and PEG6000/tetradecanol as co-porogen. These results proved the influence of the porogenic mixture composition on the monoliths' morphology. Tetradecanol-PEG shows adequately compatibility with DMSO and monomers, leading a large pore size distribution due to earlier phase separation.

Table 2
Effect of the porogen and solvent in the porous properties of NAT-ABA20-BIS.

Porogen	Solvent	Pore size (nm)[a,b]	Product yield (%)
Ethanol n-pentanol Dodecanol PEG	DMSO	< 100	80.0–85.0
Tetradecanol		690 ± 20	87.4
PEG/tetradecanol	DMAc	160 ± 30	91.0
	DMF	200 ± 80	87.6
	DMSO	1100 ± 200	90.2

[a] Pore size was estimated as the pore length of three different SEM images of each sample (mean ± SD; n° = 50).
[b] Pore sizes lower than 100 nm were not measured and correspond to an assumption than real measurement.

Fig. 6. SEM images of NAT-ABA20-BIS, using DMSO as solvent with (A) ethanol, (B) n-pentanol, (C) dodecanol, (D) tetradecanol, (E) PEG as porogen; using PEG/tetradecanol as co-porogen with (F) DMAc, (G) DMF or (H) DMSO as solvent.

Table 3
Different matrices obtained from AAc, AAm, ABA and BIS[a].

Polymer	Co-monomer (%)	ABA (%)	pore size (nm)	yield (%)	dendron incorporation (%)[b]
AAc-BIS	60	–	800 ± 200	91.2	–
AAc-ABA20-BIS	40	20	1500 ± 400	81.6	92.3
AAc-ABA30-BIS	30	30	1200 ± 90	78.6	88.2
AAc-ABA40-BIS	20	40	310 ± 80	81.9	79.7
AAm-BIS	60	–	800 ± 100	97.8	–
AAm-ABA20-BIS	40	20	1200 ± 300	89.3	81.7
AAm-ABA30-BIS	30	30	1300 ± 400	88.1	78.1
AAm-ABA40-BIS	20	40	500 ± 100	83.8	82.9

[a] Polymerization conditions: monomer concentration: 33% w/w. In all cases, 40% of BIS was used. AIBN: 1% w/w with respect to monomers. Polymerization time: 24 h; temperature: 70 °C; DMSO:co-porogen (%vol): 70:30 with respect to total volume of the porogenic mixture equal to 1 mL; co-porogen: PEG6000:tetradecanol (50:50).

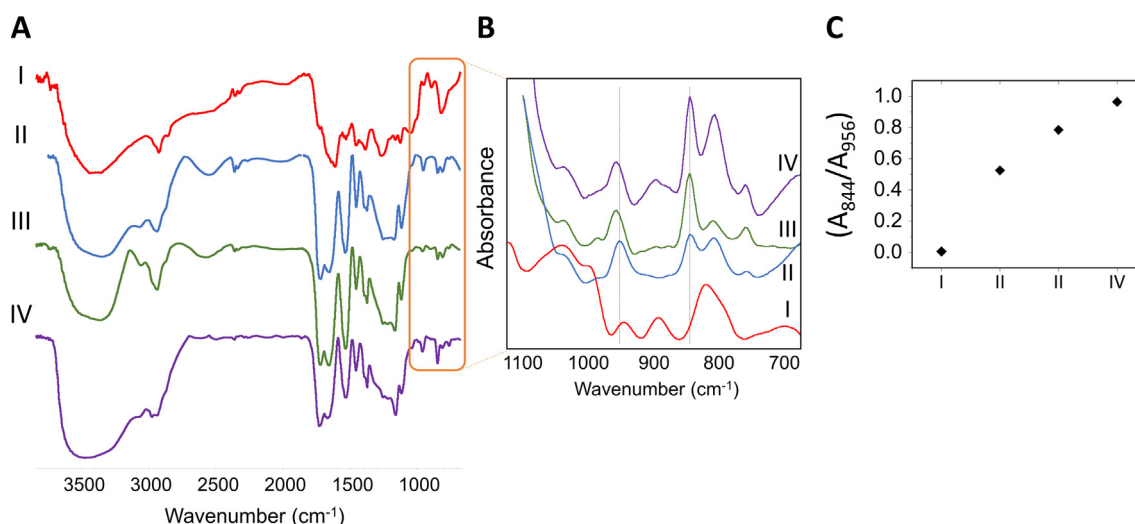[b] Percentage of mass loss from TGA graphical analysis.

Fig. 7. (A) FT-IR spectra of AAc-based matrices; (B) an expanded zone of FT-IRs; (C) relative intensity between signals at 844 and 956 cm^{-1}. (I) AAc-BIS, (II) AAc-ABA20-BIS, (III) AAc-ABA30-BIS and (IV) AAc-ABA40-BIS.

4. Conclusion

In this work, dendronized monoliths were synthesized by radical polymerization of classical monomers (NAT, AAm and AAc) with the multifunctional dendritic monomer (ABA) and the morphological characteristics were managed by the conditions of their synthesis way. The rate of polymerization and the properties of the monoliths were dependent on different variables, such as monomer, solvent, porogen, crosslinker and their ratios. According to the pore sizes distribution, the optimal monomer:crosslinker ratio was 60:40 and the higher pore size
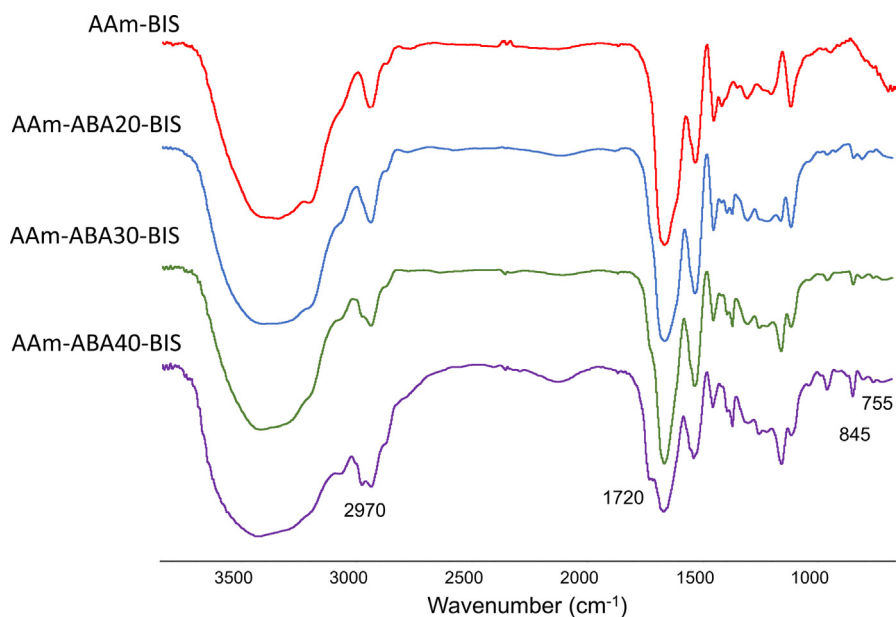
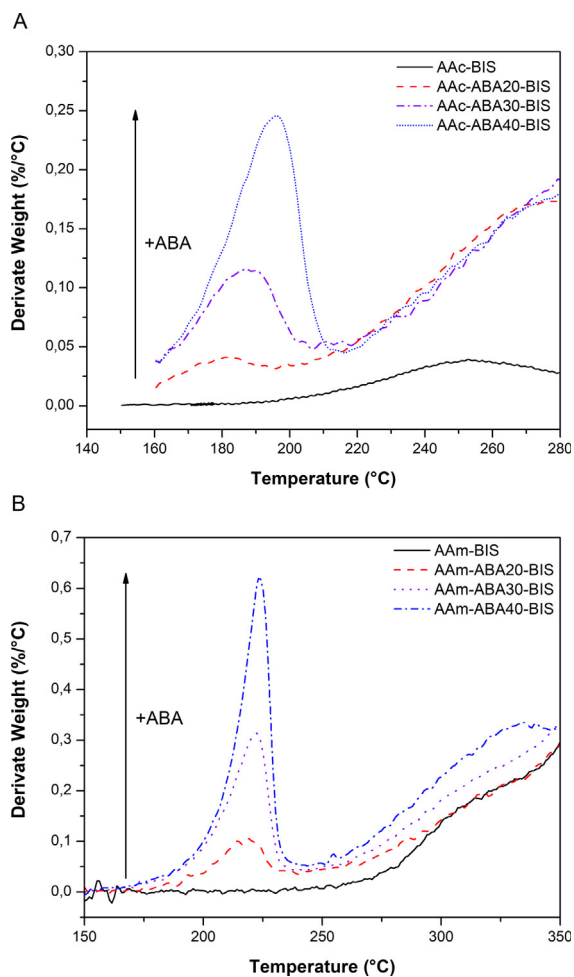**Fig. 8.** FT-IR spectra of AAm-based matrices.

Fig. 9. DTG curves of (A) AAc-based matrices and (B) AAm-based matrices of different ABA composition.

Fig. 10. Swelling percentage of (A) AAc-based and (B) AAm-based matrices in water (pH = 6.5) and DMSO.

was achieved using DMSO as solvent and PEG6000/tetradecanol as co-porogen. The AAm and AAc-based matrices showed similar morphological properties to NAT-based matrices. In all cases, the incorporation of
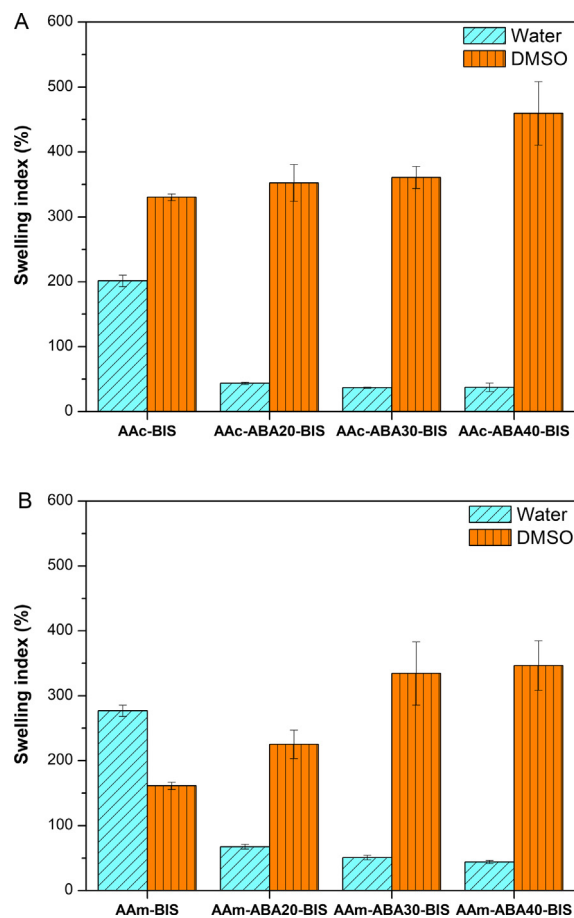
ABA decreased significantly the swelling in water due to the hydrophobic characteristic of the dendron. The monoliths showed porosity properties that depend on dendritic moiety. The pore size increased by the presence of ABA in low concentration; when de percentage of ABA increase, the pore size decreased. A high concentration of ABA (40%)
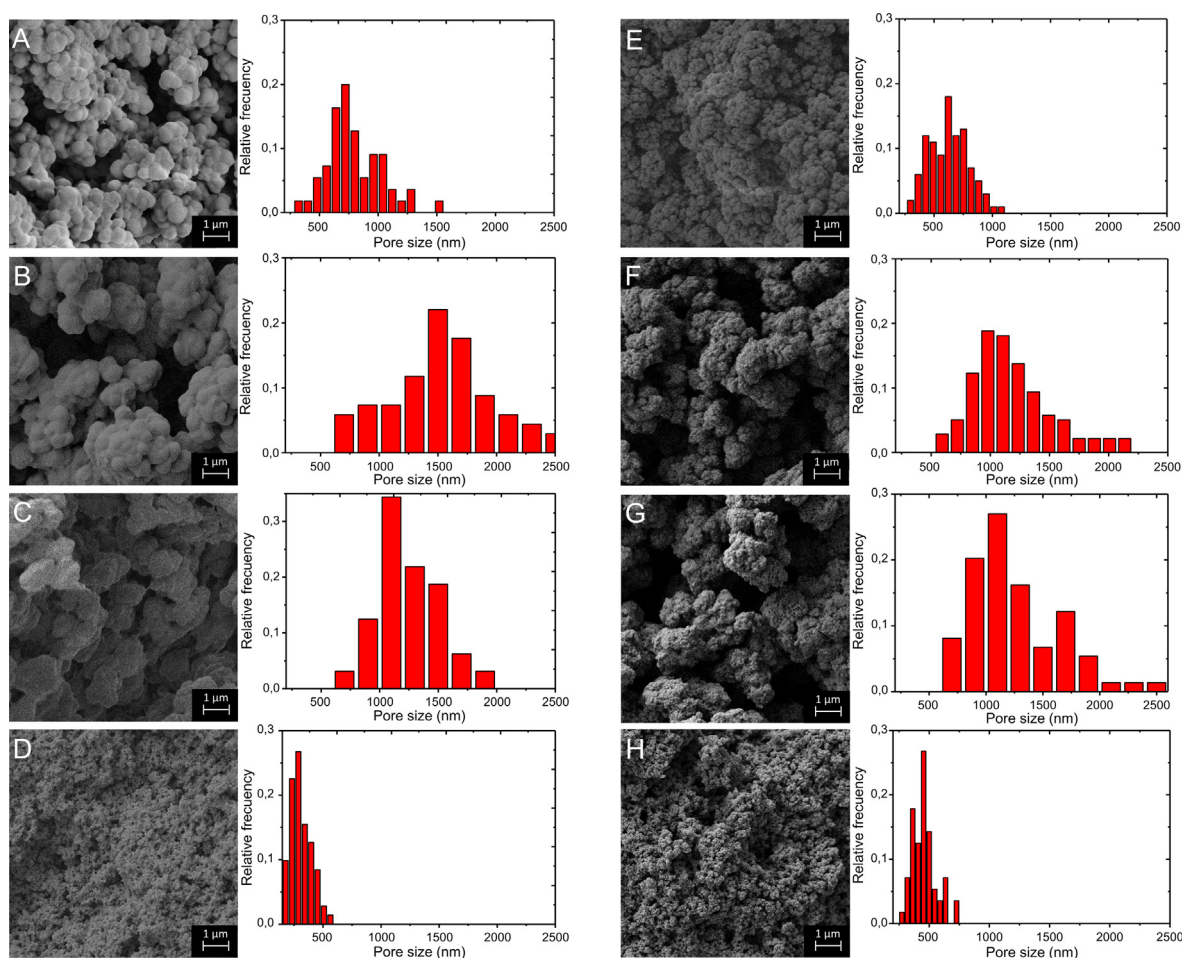
Fig. 11. SEM images and pore size distribution of: (A) AAc-BIS, (B) AAc-ABA20-BIS, (C) AAc-ABA30-BIS, (D) AAc-ABA40-BIS, (E) AAm-BIS, (F) AAm-ABA20-BIS, (G) AAm-ABA30-BIS and (H) AAm-ABA40-BIS.

results in a tight globular network with low pore size and pore volume. Thus, the dendronized monoliths improved the porous properties by using lower concentration of ABA, thus offering the opportunity to tailor pore size, morphological characteristics and pore size.

Although various modified particles with a hyperbranched structure have been used for high-performance liquid chromatography (HPLC), size exclusion chromatography (SEC), among other applications, this is the first time that dendritic-based monoliths as potential chromatography supports are reported.

Conflict of interest

The authors declare that there is no conflict of interest regarding the publication of this paper.

Acknowledgment

References

[1] R.B. Merrifield, Solid phase peptide synthesis. I. the synthesis of a tetrapeptide, J. Am. Chem. Soc. 85 (1963) 2149–2154, https://doi.org/10.1021/ja00897a025.

[2] C. Acquah, C.K.S. Moy, M.K. Danquah, C.M. Ongkudon, Development and characteristics of polymer monoliths for advanced LC bioscreening applications: a review, J. Chromatogr. B. 1015–1016 (2016) 121–134, https://doi.org/10.1016/j.jchromb.2016.02.016.

[3] T. Qi, A. Sonoda, Y. Makita, H. Kanoh, K. Ooi, T. Hirotsu, Synthesis and borate uptake of two novel chelating resins, Ind. Eng. Chem. Res. 41 (2002) 133–138, https://doi.org/10.1021/ie0104417.

[4] Z. Zajickova, Advances in the development and applications of organic–silica hybrid monoliths, J. Sep. Sci. 40 (2017) 25–48, https://doi.org/10.1002/jssc.201600774.

[5] Y. Lv, X. Tan, F. Svec, Preparation and applications of monolithic structures containing metal–organic frameworks, J. Sep. Sci. 40 (2017) 272–287, https://doi.org/10.1002/jssc.201600423.

[6] I. Nischang, T.J. Causon, Trends in analytical chemistry porous polymer monoliths: from their fundamental structure to analytical engineering applications, 75 (2016) 108–117. doi:10.1016/j.trac.2015.05.013.

[7] T.J. Causon, I. Nischang, Critical differences in chromatographic properties of silica- and polymer-based monoliths, J. Chromatogr. A. 1358 (2014) 165–171, https://doi.org/10.1016/j.chroma.2014.06.102.

[8] K.S.W. Sing, D.H. Everett, R.A.W. Haul, L. Moscou, R.A. Pierotti, J. Rouquérol, T. Siemieniewska, Reporting physisorption data for gas/solid systems with special reference to the determination of surface area and porosity (Recommendations 1984), Pure Appl. Chem. 54 (1982) 2201–2218, https://doi.org/10.1351/pac198557040603.

[9] R.D. Arrua, J.S.R. del Barrio, A.G. Ruiz, M. Strumia, C.I.A. Igarzabal, Preparation of polymeric macroporous rod systems: study of the influence of the reaction parameters on the porous properties, Mater. Chem. Phys. 112 (2008) 1055–1060, https://doi.org/10.1016/j.matchemphys.2008.07.019.

[10] A. Saeed, F. Maya, D.J. Xiao, M. Najam-ul-Haq, F. Svec, D.K. Britt, Growth of a highly porous coordination polymer on a macroporous polymer support for enhanced immobilized metal ion affinity chromatographic enrichment of phosphopeptides, Adv. Funct. Mater. 24 (2014) 5790–5797, https://doi.org/10.1002/adfm.201400116.

[11] K.J. Barlow (nee Tan), X. Hao, T.C. Hughes, O.E. Hutt, A. Polyzos, K.A. Turner, G. Moad, Porous, functional, poly(styrene-co-divinylbenzene) monoliths by RAFT

polymerization, Polym. Chem. 5 (2014) 722–732, https://doi.org/10.1039/C3PY01015E.

[12] F. Maya, F. Svec, A new approach to the preparation of large surface area poly (styrene-co-divinylbenzene) monoliths via knitting of loose chains using external crosslinkers and application of these monolithic columns for separation of small molecules, Polym. (United Kingdom) 55 (2014) 340–346, https://doi.org/10.1016/j.polymer.2013.08.018.

[13] C.T. Desire, R.D. Arrua, M. Talebi, N.A. Lacher, E.F. Hilder, Poly(ethylene glycol)-based monolithic capillary columns for hydrophobic interaction chromatography of immunoglobulin G subclasses and variants, J. Sep. Sci. 36 (2013) 2782–2792, https://doi.org/10.1002/jssc.201300558.

[14] Preparation and evaluation of 400 µm I.D. polymer-based hydrophilic interaction chromatography monolithic columns with high column efficiency, J. Chromatogr. A. 1509 (2017) 83–90. doi:10.1016/J.CHROMA.2017.06.034.

[15] T. Martinović, D. Josić, Polymethacrylate-based monoliths as stationary phases for separation of biopolymers and immobilization of enzymes, Electrophoresis 38 (2017) 2821–2826, https://doi.org/10.1002/elps.201700255.

[16] Z. Liu, J. Liu, Z. Liu, H. Wang, J. Ou, M. Ye, H. Zou, Functionalization of hybrid monolithic columns via thiol-ene click reaction for proteomics analysis, J. Chromatogr. A. 1498 (2017) 29–36, https://doi.org/10.1016/j.chroma.2017.01.029.

[17] S. Eeltink, S. Wouters, J.L. Dores-Sousa, F. Svec, Advances in organic polymer-based monolithic column technology for high-resolution liquid chromatography-mass spectrometry profiling of antibodies, intact proteins, oligonucleotides, and peptides, J. Chromatogr. A. 1498 (2017) 8–21, https://doi.org/10.1016/j.chroma.2017.01.002.

[18] M. Mammen, S.-K. Choi, G.M. Whitesides, Polyvalent interactions in biological systems: implications for design and use of multivalent ligands and inhibitors, Angew. Chem. Int. Ed. 37 (1998) 2754–2794.

[19] R. Haag, F. Kratz, Polymer therapeutics: concepts and applications, Angew. Chem. Int. Ed. 45 (2006) 1198–1215, https://doi.org/10.1002/anie.200502113.

[20] D.A. Links, The dendrimer space concept, (2012) 197–198. doi:10.1039/c1nj90060a.

[21] A.-M. Caminade, A. Ouali, R. Laurent, C.-O. Turrin, J.-P. Majoral, The dendritic effect illustrated with phosphorus dendrimers, Chem. Soc. Rev. 44 (2015) 3890–3899, https://doi.org/10.1039/C4CS00261J.

[22] S.D. Garcia Schejtman, V. Brunetti, M. Martinelli, M.C. Strumia, Chemistry of hybrid multifunctional and multibranched composites, in: V.K. Thakur, M.K. Thakur, R.K. Gupta (Eds.), Hybrid Polym. Compos. Mater., 2017, pp. 31–63. doi:10.1016/B978-0-08-100791-4.00003-3 (Chapter 3).

[23] A.A. Aldana, B. Barrios, M. Strumia, S. Correa, M. Martinelli, Dendronization of chitosan films: surface characterization and biological activity, React. Funct. Polym. 100 (2016) 18–25, https://doi.org/10.1016/j.reactfunctpolym.2016.01.003.

[24] A.A. Aldana, R. Toselli, M.C. Strumia, M. Martinelli, Chitosan films modified selectively on one side with dendritic molecules, J. Mater. Chem. 22 (2012) 22670–22677, https://doi.org/10.1039/c2jm33100d.

[25] S.D. Garcia Schejtman, R. Toselli, M.C. Strumia, M. Martinelli, Gelatin films dendronized selectively on one side: enhancing antimicrobial properties and water repellence, Polym. Bull. 72 (2015) 3043–3062, https://doi.org/10.1007/s00289-015-1452-y.

[26] A.A. Aldana, M.C. Strumia, M. Martinelli, The cooperative effect in dendronized chitosan microbeads, Aust. J. Chem. 68 (2015) 1918–1925, https://doi.org/10.1071/CH15102.

[27] M. Martinelli, M. Calderón, C.I. Alvarez I, M.C. Strumia, Functionalised supports with sugar dendritic ligand, React. Funct. Polym. 67 (2007) 1018–1026, https://doi.org/10.1016/j.reactfunctpolym.2007.06.005.

[28] J.I. Paez, M. Martinelli, V. Brunetti, M.C. Strumia, Dendronization: a useful synthetic strategy to prepare multifunctional materials, Polymers (Basel). 4 (2012) 355–395, https://doi.org/10.3390/polym4010355.

[29] H. Seto, M. Shibuya, H. Matsumoto, Y. Hoshino, Y. Miura, Glycopolymer monoliths for affinity bioseparation of proteins in a continuous-flow system: glycomonoliths, J. Mater. Chem. B. 5 (2017) 1148–1154, https://doi.org/10.1039/C6TB02930B.

[30] G.R. Newkome, K.K. Kotta, C.N. Moorefield, Convenient synthesis of 1 → 3 C-branched dendrons, J. Org. Chem. 70 (2005) 4893–4896, https://doi.org/10.1021/jo0504518.

[31] S. Brunauer, P.H. Emmett, E. Teller, Adsorption of gases in multimolecular layers, J. Am. Chem. Soc. 60 (1938) 309–319 doi:citeulike-article-id:4074706/rdoi:10.1021/ja01269a023.

[32] F.H. Ling, V. Lu, F. Svec, J.M.J. Fréchet, Effect of multivalency on the performance of enantioselective separation media for chiral HPLC prepared by linking multiple selectors to a porous polymer support via aliphatic dendrons, J. Org. Chem. 67

(2002) 1993–2002, https://doi.org/10.1021/jo011005x.

[33] J.C. Cuggino, M. Calderon, C.I. Alvarez, M.C. Strumia, K.N. Silva, E.K. Penott-Chang, A.J. Muller, New dendronized polymers from acrylate Behera amine and their ability to produce visco-elastic structured fluids when mixed with CTAT worm-like micelles, J. Colloid Interface Sci. 357 (2011) 147–156, https://doi.org/10.1016/j.jcis.2011.01.075.

[34] J. Huang, X. Zhou, A. Lamprou, F. Maya, F. Svec, S.R. Turner, Nanoporous polymers from cross-linked polymer precursors via tert-Butyl group deprotection and their carbon dioxide capture properties, Chem. Mater. 27 (2015) 7388–7394, https://doi.org/10.1021/acs.chemmater.5b03114.

[35] G.N. Rimondino, E. Miceli, M. Molina, S. Wedepohl, S. Thierbach, E. Rühl, M. Strumia, M. Martinelli, M. Calderón, Rational design of dendritic thermo-responsive nanogels that undergo phase transition under endolysosomal conditions, J. Mater. Chem. B. 5 (2017) 866–874, https://doi.org/10.1039/C6TB02001A.

[36] F. Svec, J.M.J. Frechet, Kinetic control of pore formation in macroporous polymers. Formation of "molded" porous materials with high flow characteristics for separations or catalysis, Chem. Mater. 7 (1995) 707–715, https://doi.org/10.1021/cm00052a016.

[37] R.D. Arrua, C.I. Alvarez Igarzabal, Macroporous monolithic supports for affinity chromatography, J. Sep. Sci. 34 (2011) 1974–1987, https://doi.org/10.1002/jssc.201100197.

[38] B.P. Santora, M.R. Gagne, K.G. Moloy, N.S. Radu, Porogen and cross-linking effects on the surface area, pore volume distribution, and morphology of macroporous polymers obtained by bulk polymerization, Macromolecules 34 (2001) 658–661, https://doi.org/10.1021/ma0004817.

[39] R.D. Arrua, C. Moya, E. Bernardi, J. Zarzur, M. Strumia, C.I.A. Igarzabal, Preparation of macroporous monoliths based on epoxy-bearing hydrophilic terpolymers and applied for affinity separations, Eur. Polym. J. 46 (2010) 663–672, https://doi.org/10.1016/j.eurpolymj.2010.01.009.

[40] H. Esen, Synthesis and characterization of linear dendritic homo and copolymers acrylated behera amine, Des. Monomers Polym. 18 (2015) 745–752, https://doi.org/10.1080/15685551.2015.1070506.

[41] R. Dong, Y. Zhou, X. Zhu, Supramolecular dendritic polymers: from synthesis to applications, Acc. Chem. Res. 47 (2014) 2006–2016, https://doi.org/10.1021/ar500057e.

[42] A. Zhang, L. Okrasa, T. Pakula, A.D. Schlüter, Homologous series of dendronized polymethacrylates with a methyleneoxycarbonyl spacer between the backbone and dendritic side chain: synthesis, characterization, and some bulk properties, J. Am. Chem. Soc. 126 (2004) 6658–6666, https://doi.org/10.1021/ja0494205.

[43] M.K. Danquah, G.M. Forde, Preparation of macroporous methacrylate monolithic material with convective flow properties for bioseparation: Investigating the kinetics of pore formation and hydrodynamic performance, Chem. Eng. J. 140 (2008) 593–599, https://doi.org/10.1016/j.cej.2008.02.012.

[44] R.J. Vonk, S. Wouters, A. Barcaru, G. Vivo-Truyols, S. Eeltink, L.J. de Koning, P.J. Schoenmakers, Post-polymerization photografting on methacrylate-based monoliths for separation of intact proteins and protein digests with comprehensive two-dimensional liquid chromatography hyphenated with high-resolution mass spectrometry, Anal. Bioanal. Chem. (2015) 3817–3829, https://doi.org/10.1007/s00216-015-8615-4.

[45] L. Chen, J. Ou, Z. Liu, H. Lin, H. Wang, J. Dong, H. Zou, Fast preparation of a highly efficient organic monolith via photo-initiated thiol-ene click polymerization for capillary liquid chromatography, J. Chromatogr. A. 1394 (2015) 103–110, https://doi.org/10.1016/j.chroma.2015.03.054.

[46] S. Xie, F. Svec, J.M.J. Frechet, Preparation of porous hydrophilic monoliths: effect of the polymerization conditions on the porous properties of poly (acrylamide-co-N,N-methylenebisacrylamide) monolithic rods, J. Polym. Sci. Part A Polym. Chem. 35 (1997) 1013–1021, https://doi.org/10.1002/(SICI)1099-0518(19970430)35:6<1013::AID-POLA4>3.0.CO;2-5.

[47] D. Hoegger, R. Freitag, Acrylamide-based monoliths as robust stationary phases for capillary electrochromatography, J. Chromatogr. A. 914 (2001) 211–222, https://doi.org/10.1016/S0021-9673(00)01119-5.

[48] D.S. Peterson, T. Rohr, F. Svec, J.M.J. Fréchet, Enzymatic microreactor-on-a-chip: protein mapping using trypsin immobilized on porous polymer monoliths molded in channels of microfluidic devices, Anal. Chem. 74 (2002) 4081–4088, https://doi.org/10.1021/ac020180q.

[49] J.B. Qu, Y.D. Huang, G.L. Jing, J.G. Liu, W.Q. Zhou, H. Zhu, J.R. Lu, A novel matrix derivatized from hydrophilic gigaporous polystyrene-based microspheres for high-speed immobilized-metal affinity chromatography, J. Chromatogr. B Anal. Technol. Biomed. Life Sci. 879 (2011) 1043–1048, https://doi.org/10.1016/j.jchromb.2011.03.015.